Elastic collisions among peakon solutions for the Camassa–Holm equation

Alina Chertock [a], Jian-Guo Liu [b], Terrance Pendleton [c]

[a] Department of Mathematics, North Carolina State University, Raleigh, NC 27695, USA
[b] Department of Physics and Department of Mathematics, Duke University, Durham, NC 27708, USA
[c] Department of Mathematics, Iowa State University, Ames, IA 50010, USA

ARTICLE INFO

Article history:
Available online 24 January 2014

Keywords:
Camassa–Holm equation
Particle method
Peakon solutions
Elastic collisions
Conservation laws
Completely integrable systems

ABSTRACT

The purpose of this paper is to study the dynamics of the interaction among a special class of solutions of the one-dimensional Camassa–Holm equation. The equation yields soliton solutions whose identity is preserved through nonlinear interactions. These solutions are characterized by a discontinuity at the peak in the wave shape and are thus called peakon solutions. We apply a particle method to the Camassa–Holm equation and show that the nonlinear interaction among the peakon solutions resembles an elastic collision, i.e., the total energy and momentum of the system before the peakon interaction is equal to the total energy and momentum of the system after the collision. From this result, we provide several numerical illustrations which support the analytical study, as well as showcase the merits of using a particle method to simulate solutions to the Camassa–Holm equation under a wide class of initial data.

1. Introduction

The purpose of this paper is to investigate the dynamics of the interaction among peakon solutions for the one-dimensional (1-D) Camassa–Holm (CH) equation as well as showcase the merits of using particle methods to simulate solutions to the CH equation using arbitrary smooth initial data. To this extent, the CH equation is given by

$$m_t + um_x + 2mu_x = 0, \quad m = u - \alpha^2 u_{xx}, \tag{1}$$

which is subjected to the following initial data:

$$m(x,0) = m_0(x). \tag{2}$$

Here, m is the momentum related to the fluid velocity u by the 1-D Helmholtz operator (see (1)).

Eq. (1) arises in a wide range of scientific applications and, for example, can be described as a bi-Hamiltonian model in the context of shallow water waves, see [2,14,15]. It can also be used to quantify growth and other changes in shape, such as those which occur in a beating heart, by providing the transformative mathematical path between two shapes (for instance, see [21] p. 420).

The CH equation exhibits some interesting properties among a class of nonlinear evolutionary PDEs. For instance, the equation is completely integrable and thus possesses an infinite number of conservation laws. Eq. (1) yields soliton solutions—whose identity is preserved through nonlinear interactions—which are characterized by a discontinuity at the peak in the wave shape., see, e.g. [2,4,27]. More precisely, Eq. (1) admits traveling wave solutions of the form

E-mail addresses: chertock@math.ncsu.edu (A. Chertock), Jian-Guo.Liu@duke.edu (J.-G. Liu), tlpendle@iastate.edu (T. Pendleton).

0168-9274/$36.00
http://dx.doi.org/10.1016/j.apnum.2014.01.001

$u(x,t) = ae^{-|x-ct|}$ with speed proportional to amplitude. For these reasons, soliton solutions generated from the CH equation are referred to as peakons. Peakons are also orbitally stable as their shape is maintained under small perturbations; see, e.g. [16,25,17].

Simulating these peakon solutions numerically poses quite a challenge—especially if one is interested in considering a peakon–antipeakon interaction (i.e., the interaction between positive and negative peakons). Several sophisticated numerical methods in finite-difference, finite-element, and spectral settings have been proposed for accurately resolving the CH equation—in particular, peakon interactions. For example, in [18], a self-adaptive mesh method was proposed, whereas in [22,23], a spectral projection method was used to simulate solutions to the CH equation. In [13], the authors used multi-symplectic integration, and in [26], an energy-conserving Galerkin scheme was proposed. In [12], the authors considered a dispersion-relation-preserving algorithm. For additional numerical schemes proposed for solving the CH equation, we refer the reader to [1,3,20,29,30] and references therein. Many of these methods are computationally intensive and require very fine grids along with adaptivity techniques in order to model the peakon behavior. Moreover, many of these methods are unable to successfully resolve the peakon–antipeakon interaction.

Solutions of (1), (2) can be accurately captured by using a particle method, as shown in [20,10,5,6]. In the particle method, described in [10,6,11], the solution is sought as a linear combination of Dirac distributions, whose positions and coefficients represent locations and weights of the particles, respectively. The solution is then found by following the time evolution of the locations and the weights of these particles according to a system of ODEs obtained by considering a weak formulation of the problem. The particle methods presented in [5,6] have been derived using a discretization of a variational principle and provide the equivalent representation of the ODE particle system. The main advantage of particle methods is their (extremely) low numerical diffusion that allows one to capture a variety of nonlinear waves with high resolution; see, e.g., [7–9,28] and references therein.

In this paper, we apply the particle method for the numerical solution of the CH equation in order to study the elastic collisions among peakon solutions. We begin, in Section 2, with a brief overview of the particle method and some of its main properties which are necessary for the study of numerical collisions among peakon solutions. We then provide in Section 3 an analytical discussion about the behavior of peakon interactions for two positive peakons. Finally, in Section 4, we present several numerical experiments which showcase both the complex interactions among peakon solutions, as well as the merits of using a particle method to simulate such solutions.

2. Description of the particle method for the Camassa–Holm equation

In this section, we briefly describe a particle method for the CH equation. For a more detailed description on the particle method for (1), we refer the reader to [10,11,6]. We begin by searching for a weak solution in the form of a linear combination of Dirac delta distributions. In particular, we look for a solution of the form:

$$m^N(x,t) = \sum_{i=1}^{N} p_i(t)\delta\big(x - x_i(t)\big). \tag{3}$$

Here, $x_i(t)$ and $p_i(t)$ represent the location of the i-th particle and its weight, and N denotes the total number of particles. The solution is then found by following the time evolution of the locations and the weights of the particles according to the following system of ODEs:

$$\begin{cases} \dfrac{dx_i(t)}{dt} = u\big(x_i(t),t\big), & i = 1,\dots,N, \\ \dfrac{dp_i(t)}{dt} + u_x\big(x_i(t),t\big)p_i(t) = 0, & i = 1,\dots,N. \end{cases} \tag{4}$$

Using the special relationship between m and u given in (1), one can directly compute the velocity u and its derivative, by the convolution $u = G * m$, where G is the Green's function

$$G\big(|x-y|\big) = \frac{1}{2\alpha}e^{-|x-y|/\alpha}, \tag{5}$$

associated with the one-dimensional Helmholtz operator in (1). Thus we have the following exact expressions for both $u(x,t)$ and (by direct computation) $u_x(x,t)$:

$$u^N(x,t) = \big(m^N * G\big)(x,t) = \frac{1}{2\alpha}\sum_{i=1}^{N} p_i(t)e^{-|x-x_i(t)|/\alpha}, \tag{6}$$

$$u_x^N(x,t) = \big(m^N * G_x\big)(x,t) = -\frac{1}{2\alpha^2}\sum_{i=1}^{N} p_i(t)\,\mathrm{sgn}\big(x-x_i(t)\big)e^{-|x-x_i(t)|/\alpha}. \tag{7}$$

To initialize the particle method for the CH equation, one should choose the initial positions of particles, $x_i(0)$, and the weights, $p_i(0)$, so that (3) represents a high-order approximation to the initial data $m_0(x)$ in (1). The latter can be done in

the sense of measures on $\mathbb{R}$. Namely, we choose $(x_i(0), p_i(0))$ in such a way that for any test function $\phi(x) \in C_0^\infty(\mathbb{R})$, we have that

$$\left\langle m_0^N(\cdot), \phi(\cdot)\right\rangle = \int_{\mathbb{R}} m_0(x)\phi(x)\,dx \approx \sum_{i=1}^{N} p_i(0)\phi(x_i), \tag{8}$$

where

$$m_0^N(x) = \sum_{i=1}^{N} p_i(0)\delta\big(x - x_i(0)\big). \tag{9}$$

Based on (8), we observe that determining the initial weights, $p_i(0)$, are exactly equivalent to solving a standard numerical quadrature problem. One way of solving this problem is to cover the computational domain Ω with a uniform mesh of spacing Δx and denote by Ω_i the interval

$$\Omega_i = [x_{i-1/2}, x_{i+1/2}] = \{x \mid x_{i-1/2} \leqslant x \leqslant x_{i+1/2}\}, \quad i = 1, \ldots, N,$$

and by $x_i(0) = i\Delta x$ the center Ω_i. For example, a midpoint quadrature will then be given by setting $p_i(0) = \Delta x\, m_0(x_i(0))$. In general, one can build a sequence of basis functions $\{\varphi_i(x)\}_{i=1}^N$ and approximate the initial data by taking $p_i(0) = \int_{\mathbb{R}} \varphi_i(x)\,dm_0$ in (9). Note that the latter makes sense if $m_0 \in \mathcal{M}(\mathbb{R})$, where $\mathcal{M}(\mathbb{R})$ is the set of Radon measures and one can prove that m_0^N converges weakly to $m_0(x)$ as $N \to \infty$.

In practice, except for very special cases, the functions $x_i(t)$ and $p_i(t)$, $i = 1, \ldots, N$, have to be determined numerically and the system (4) must be integrated by an appropriate ODE solver. For our numerical experiments, we considered a strong-stability preserving (SSP) Runge–Kutta method from [19]. For a more complete description of this method, we refer the reader to Appendix A.

It should be observed that once the positions, x_i, of the particles and their weights, p_i, are obtained from (4), the solution at any point can be easily computed using (6). Furthermore, if the initial data assumes the form of a peakon, then the peakon solution generated by the particle method is exact, with any errors emanating solely from the ODE solver.

2.1. Properties of the particle system

It should be instructive to discuss some of the general properties of the particle system which are pertinent to our study on the investigation of elastic collisions of peakons. For a more detailed description of the following properties including their proofs, we refer the reader to [10,11].

- We begin by observing that the functions $x_i(t)$ and $p_i(t)$ given by (4) satisfy the following canonical Hamiltonian equations:

$$\frac{dx_i}{dt} = \frac{\partial H^N}{\partial p_i}, \qquad \frac{dp_i}{dt} = -\frac{\partial H^N}{\partial x_i}, \quad i = 1, \ldots, n, \tag{10}$$

  where the Hamiltonian $H^N(t)$ is given as follows:

$$H^N(t) = \frac{1}{2}\sum_{i=1}^{N}\sum_{j=1}^{N} p_i(t)p_j(t)G\big(x_i(t) - x_j(t)\big), \tag{11}$$

  where G is given in (5). We note that $H^N(t)$ is conserved, i.e., $H^N(t) = H^N(0)$ for all $t > 0$.
- Another important conservation law for the particle system (4) is the conservation of the total momentum, i.e.,

$$\frac{d}{dt}\left[\sum_{i=1}^{N} p_i(t)\right] = 0. \tag{12}$$

- Finally, if the initial momenta given in (4) are positive, i.e., $p_i(0) > 0$ for all $i = 1, \ldots, N$, then $p_i(t) > 0$ for all $i = 1, \ldots, N$ and $t > 0$. If, in addition, $x_i(0) < x_{i+1}(0)$, $i = 1, \ldots, N$, then the particles never cross, i.e., $x_i(t) < x_{i+1}(t)$ for any $i = 1, \ldots, N$ and for all t. This important property was proved in [5] by using a Lax–Pair formulation. It can also be proved by using a conservation law,

$$\frac{dP_N(t)}{dt} := \frac{d}{dt}\left(\prod_{k=1}^{N} p_k(t)\prod_{k=1}^{N-1}\big[G(0) - G\big(x_k(t) - x_{k+1}(t)\big)\big]\right) = 0,$$

  as it has been done in [11]. We will show in the next section, the peakon particles indeed elastically bounce back after becoming close to each other.

3. Elastic collisions among peakon solutions

In this section, we take a close look at the dynamics and interactions of the peakon solutions (6) associated with CH equation. In particular, we study the soliton-type behavior of peakons and their elastic collisions. An elastic collision is an encounter between two bodies in which the total kinetic energy and momentum of the two bodies after the encounter are equal to their total kinetic energy and momentum before the encounter. That is, both momentum and kinetic energy are conserved. By conservation of momentum, we mean that the sum of the momenta of all the objects of a system under consideration cannot be changed by the interactions within the system. Additionally, the total energy of a system remains constant at all times under the conservation of energy principle. Using these principal conservation properties, we begin by showing analytically that any collisions among peakons for the case where the initial weights are assumed to be positive are elastic. The collision is through the interaction potential in the Hamiltonian given in (10) rather than a head on collision.

3.1. Analysis of two-peakon interactions

Since the interaction of peakons is local, it is sufficient to investigate the interactions among two peakons. To this extent, we consider a two-peakon system with weights $p_1(t)$, $p_2(t)$ and locations $x_1(t)$, $x_2(t)$ that evolve in time according to the following system of ODEs (see (4)):

$$\begin{cases} \dfrac{dx_1(t)}{dt} = \dfrac{1}{2\alpha}p_1(t) + \dfrac{1}{2\alpha}p_2(t)e^{-|x_2(t)-x_1(t)|/\alpha}, \\ \dfrac{dx_2(t)}{dt} = \dfrac{1}{2\alpha}p_2(t) + \dfrac{1}{2\alpha}p_1(t)e^{-|x_1(t)-x_2(t)|/\alpha}, \\ \dfrac{dp_1(t)}{dt} = \dfrac{1}{2\alpha^2}p_1(t)p_2(t)\,\mathrm{sgn}\big(x_1(t)-x_2(t)\big)e^{-|x_1(t)-x_2(t)|/\alpha}, \\ \dfrac{dp_2(t)}{dt} = \dfrac{1}{2\alpha^2}p_1(t)p_2(t)\,\mathrm{sgn}\big(x_2(t)-x_1(t)\big)e^{-|x_2(t)-x_1(t)|/\alpha}. \end{cases} \tag{13}$$

We assume that there are two times, say t_{before} and t_{after} such that $|x_1(t_{\text{before}}) - x_2(t_{\text{before}})| = |x_1(t_{\text{after}}) - x_2(t_{\text{after}})|$ with $x_1(t) \neq x_2(t)$ for any finite time t. Here t_{before} is some time t before the two peakons interact, and t_{after} is some time t after the peakons undergo a nonlinear exchange of momentum.

We begin by recalling the two conservation properties of the particle system given in Section 2: The conservation of the Hamiltonian (see (10)):

$$H^N(t) = p_1^2(t) + p_2^2(t) + 2p_1(t)p_2(t)e^{-|x_1(t)-x_2(t)|/\alpha} = H^N(0), \quad \forall t > 0, \tag{14}$$

and the conservation of momentum (see (12)):

$$p_1(t) + p_2(t) = p_1(0) + p_2(0), \quad \forall t > 0. \tag{15}$$

From (14) and (15), we observe that $2(p_1p_2)_{\text{before}} = 2(p_1p_2)_{\text{after}}$. Indeed if we square both sides of (15) and subtract (14), we obtain

$$2p_1(t_{\text{before}})p_2(t_{\text{before}})\big(1 - e^{-|x_1(t_{\text{before}})-x_2(t_{\text{before}})|/\alpha}\big) = 2p_1(t_{\text{after}})p_2(t_{\text{after}})\big(1 - e^{-|x_1(t_{\text{after}})-x_2(t_{\text{after}})|/\alpha}\big).$$

From here, we use the fact that $|x_1(t_{\text{before}}) - x_2(t_{\text{before}})| = |x_1(t_{\text{after}}) - x_2(t_{\text{after}})|$ to conclude that $2(p_1p_2)_{\text{before}} = 2(p_1p_2)_{\text{after}}$. This observation along with the conservation of momentum property (see (15)) allows us to obtain the following system of equations:

$$\begin{aligned} &p_1^2(t_{\text{before}}) + p_2^2(t_{\text{before}}) = p_1^2(t_{\text{after}}) + p_2^2(t_{\text{after}}), \\ &p_1(t_{\text{before}}) + p_2(t_{\text{before}}) = p_1(t_{\text{after}}) + p_2(t_{\text{after}}). \end{aligned} \tag{16}$$

The only possible solutions to the system of equation given above are,

$$p_1(t_{\text{before}}) = p_1(t_{\text{after}}), \qquad p_2(t_{\text{before}}) = p_2(t_{\text{after}}), \tag{17}$$

and

$$p_1(t_{\text{before}}) = p_2(t_{\text{after}}), \qquad p_2(t_{\text{before}}) = p_1(t_{\text{after}}). \tag{18}$$

The solution given by (17) implies that the peakons do not interact, which is not possible. Hence, the solution to (16) is given by (18) which shows that the momentum is exchanged after the collision. This explicitly shows the elastic collision behavior among peakon solutions generated by solving (1) via a particle method. Below, we illustrate an example of the interaction among two peakons which exhibits the elastic collision behavior as described above.

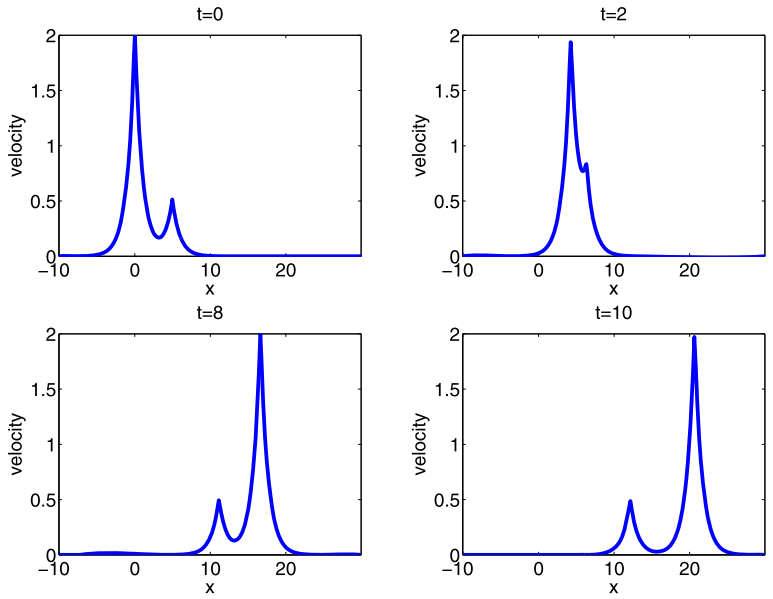

Fig. 1. Two positive peakon interaction for the CH equation (1) for various times.

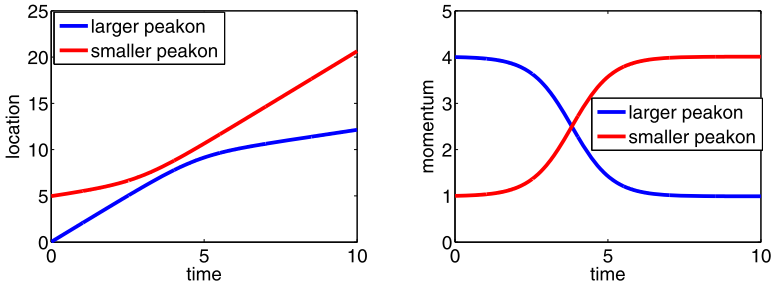

Fig. 2. Location and momentum trajectories for the two positive peakon interaction.

3.1.1. An illustration of the two positive peakon interaction

In this illustration, we begin by considering an interaction among two positive peakons generated from solving the CH equation given in (1). To this extent, we consider two positive peakons, which are initially placed at $x_1(0) = 0$, and $x_2(0) = 5$ with initial weights $p_1(0) = 4$ and $p_2(0) = 1$, and move them exactly in time according to (13) with $\alpha = 1$ on the domain $[a, b] = [-10, 30]$. We observe that the peakon defined by its initial values at (x_1, p_1) has a bigger weight and will hence move faster than the peakon defined by (x_2, p_2). Thus, we expect that as the two peakons move closer to each other, they will undergo a complex interaction which involves the exchange of momentum.

In Fig. 1, we provide snapshots of the solution u at different times. To plot the velocity profile, we introduce a uniform grid of size Δx^p, i.e., $x_j^p = j\Delta x^p$, $\Delta x^p = \frac{b-a}{N_p}$, $j = 1, \ldots, N_p$, and compute the values of $u(x_j^p, t)$, $j = 1, \ldots, N_p$, according to formula (6) with $\alpha = 1$, i.e., $u^N(x_j^p, t) = \frac{1}{2}\sum_{i=1}^{N_p} p_i(t) e^{-|x_j^p - x_i(t)|}$ where the superscript p denotes the particle method. As one can see, the peakons emerge unscathed with the exception of a phase shift as predicted by the underlying integrable system. In Fig. 2, we also show the trajectories of each particle and its momentum as functions of time. From this figure, we see that the particles do not cross; rather, they exchange momentums as they undergo a complex nonlinear interaction with each other.

To gain a better understanding of the elastic collision behavior among two peakon solutions, we compare the particle method (13), in which each particle represents a peakon with the multi-particle approach for simulating the evolution of two peakons. The latter case assumes a simple form as well. We follow the method presented in [10] and consider a suitably refined initial grid of particles to represent the two peakons, in which the initial weights, p_i, of the particles are all zero except for two particles that initially have weights $p_{n_1}(0) = 4$ and $p_{n_2}(0) = 1$ and are placed at $x_{n_1}(0) = 0$ and $x_{n_2}(0) = 5$, respectively. In this case, it follows from (4) that $dp_i/dt = 0$ for each $i \neq n_1, n_2$, and thus the weights of all of the weightless particles will remain constant in time. However, the locations of these particles may change in time since the velocity of the particles depend explicitly on (6) which is not necessarily zero. From (4) and (6), we observe that the $u(x_i(t), t)$ depends solely on $x_{n_1}(t), x_{n_2}(t)$ and $p_{n_1}(t), p_{n_2}(t)$, and thus it is sufficient to evolve the same ODEs for non-zero particles as before.

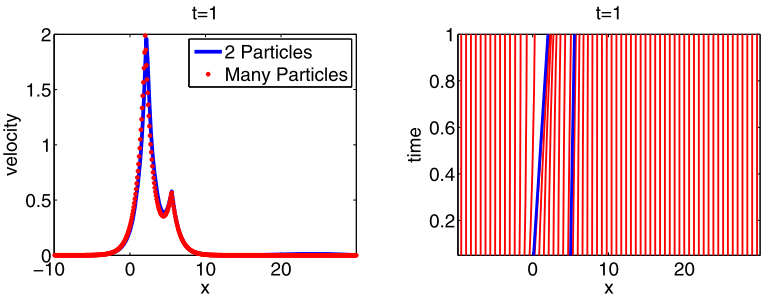

Fig. 3. The velocity u for the CH equation (1) at $t = 1$, and the associated particle location trajectories. (For interpretation of the references to color in this figure, the reader is referred to the web version of this article.)

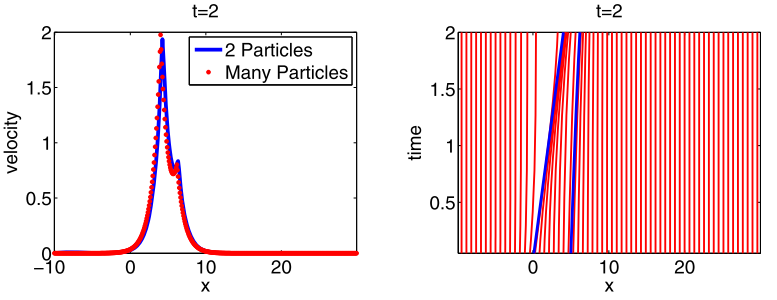

Fig. 4. The velocity u for the CH equation (1) at $t = 2$, and the associated particle location trajectories. (For interpretation of the references to color in this figure, the reader is referred to the web version of this article.)

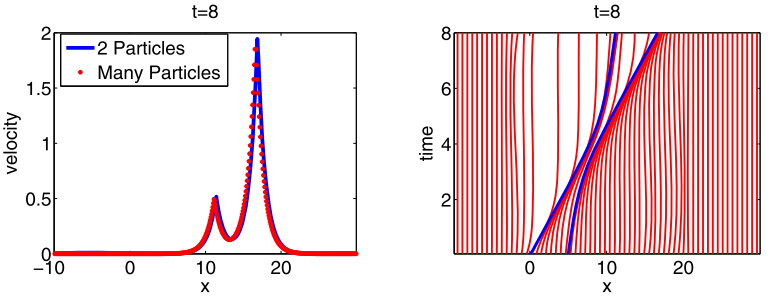

Fig. 5. The velocity u for the CH equation (1) at $t = 8$, and the associated particle location trajectories. (For interpretation of the references to color in this figure, the reader is referred to the web version of this article.)

To rectify the issue of particles clustering around each other, we implement a swapping algorithm, in which the particles are switched once a certain distance threshold is met. In particular, if as before we let Δx^p be the distance between each equidistant point on a computational grid, then we switch the weights, $p_{i+1}(t) \leftrightarrow p_i(t)$, if $x_{i+1}(t) - x_i(t) < \min(\frac{1}{2}(x_i(t) - x_{i-1}(t)), \frac{1}{2}\Delta x^p)$, and $p_i(t) \geqslant p_{i+1}(t)$. Physically, this algorithm allows peakons to undergo a complex, nonlinear interaction for which there is an exchange of momentum. The results are shown in Figs. 3–6—the blue lines correspond to the solution (trajectories) obtained by running the two particles system (13), while the red ones correspond to solution computed using the multi-particle approach according to the system (4). Once again, to plot the computed solution $u(x, t)$, we recover its values on a uniform grid using (6). As one can see, the trajectory paths with many particles agree with the trajectory paths for the solution in which we consider only two particles. This shows that even when we consider the interaction among many particles in a peakon simulation, the particle will never cross; rather, they exchange momentums as the particles move closer to each other.

3.1.2. An illustration of the peakon–antipeakon interaction

One may also observe this no crossing behavior in the peakon–antipeakon case. In this illustration (Fig. 7), the peakon and antipeakon (a peakon with a negative initial weight) are initially located at $x_{n_1}(0) = -10$ and $x_{n_2}(0) = 10$ and have momenta of equal magnitude but opposite signs so that the total momentum is zero, i.e., $p_{n_1}(0) = 1$ and $p_{n_2}(0) = -1$. We move the peakons exactly in time according to (13) with $\alpha = 1$ on the domain $[a, b] = [-30, 30]$. During the simulation, the total momentum remains zero, however the magnitudes grow very large as the peakon traveling from the left to the

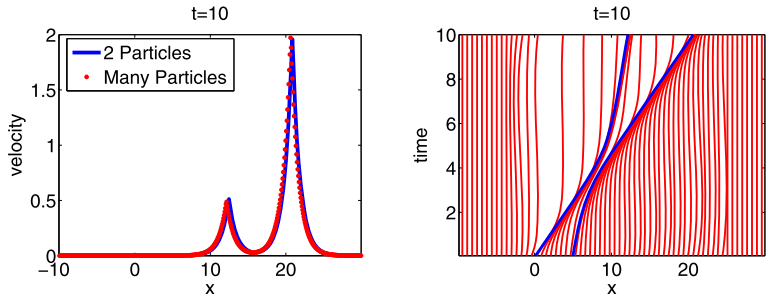

Fig. 6. The velocity u for the CH equation at $t = 10$, and the associated particle location trajectories. (For interpretation of the references to color in this figure, the reader is referred to the web version of this article.)

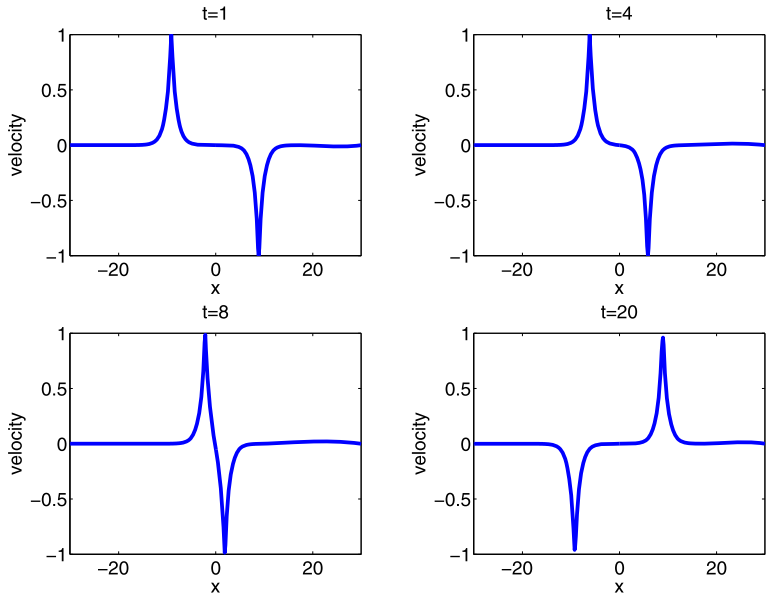

Fig. 7. An Illustration of the peakon–antipeakon phenomenon at various times.

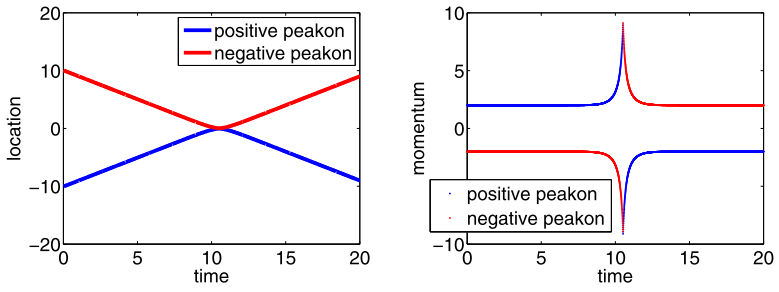

Fig. 8. Location and momentum trajectories for the peakon–antipeakon interaction.

right approaches the antipeakon traveling in the opposite direction. At some finite time, t^*, the peakon and antipeakon will collide. Since the total momentum of the system is zero, we expect that the solution will be zero at the collision time t^*. However, due to the inherent symmetry of the problem, $u(x,t) \to -u(-x,-t)$ (cf., [10] and references therein), peakons may develop after the collision time and propagate in opposite directions, thus exhibiting the elastic collision properties discussed in the previous section. To implement this numerically, we allow particles to exchange momentum, if the particles associated with the nonzero weights are sufficiently close to each other, i.e. $|x_{n_1} - x_{n_2}| < d^*$ where d^* is some prescribed small distance. In our examples, $d^* = \frac{1}{2}\Delta x^p$. To recover the solution $u(x,t)$ as shown below, we once again calculate its values on a uniform grid according to (6) (as before, we take $x_j^p = j\Delta x^p$, $\Delta x^p = \frac{b-a}{N_p}$). In Figs. 8 and 9 we plot the location and momentum trajectories for the peakon and antipeakon as a function of time. Here, we observe that similar

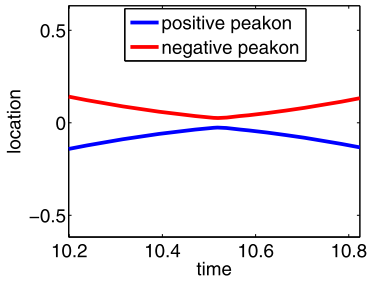

Fig. 9. (Zoomed) Location trajectories for the peakon–antipeakon interaction.

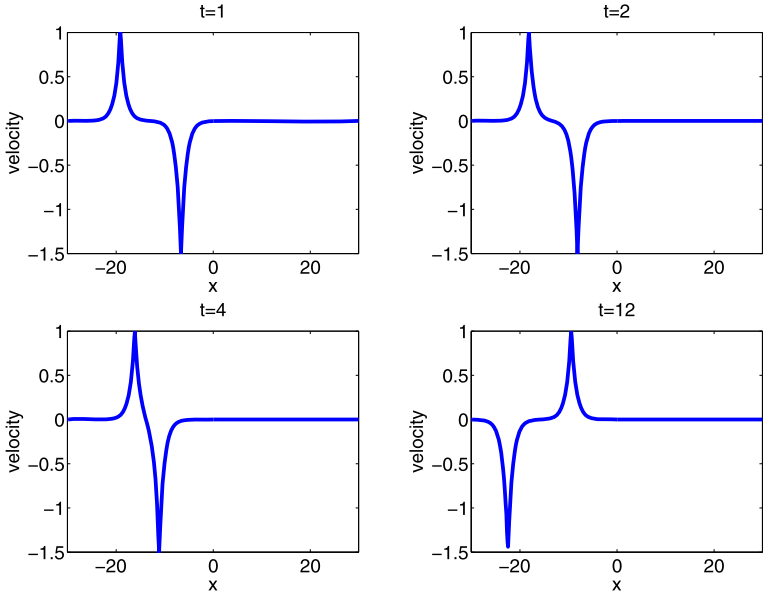

Fig. 10. An Illustration of the peakon–antipeakon (with different magnitudes) phenomenon at various times.

to the two positive peakon example, the collision between the peakon and antipeakon is elastic in the sense that it involves the exchange of momentum.

If we consider the example where the peakon and antipeakon do not have weights with the same magnitude (say, $p_{n_1}(0) = 1$ and $p_{n_2}(0) = -1.5$), then one may also observe the no crossing behavior for which the peakons exchange momentum. We solve the problem exactly as above with the only change being in the initial weights. With this change, the total momentum is no longer 0; rather, it is -0.5. Similar to the example above, the magnitudes grow very large as the peakon traveling from the left to the right approaches the antipeakon traveling in the opposite direction. Once again, at some finite time, t^*, the peakon and antipeakon will collide. This time, however, the two peakons merge into one antipeakon with a weight -0.5 which is to be expected. Taking advantage of the inherent symmetry built into the problem (see above), we know that peakons may develop after the collision and propagate in different directions. Using the same numerical strategy as the first peakon–antipeakon example, we observe that the collision between the peakon and antipeakon is elastic in the sense that it involves the exchange of momentum, even when the initial weights have different magnitudes. See Figs. 10–12.

4. Numerical experiments

In this section, we perform several numerical simulations, which solve the CH equation under a wide range of initial data. We illustrate that the peakons' behavior is reminiscent of the soliton paradigm as the peakon represents a self-reinforcing solitary wave that maintains its shape while it travels at a constant finite speed. Peakons also exhibit remarkable stability as their identity is retained through strong nonlinear interactions. The presented numerical examples do not only corroborate the analytical results, but also demonstrate some of the practical advantages that the particle method holds over other numerical methods. In particular, we consider both peakon solutions and solutions arising from arbitrary smooth (and non-smooth) initial data. In all cases, we compare the results obtained by the particle method (PM) with those obtained using a finite volume (FV) approach, in particular, a semi-discrete central upwind scheme described in Appendix A (see

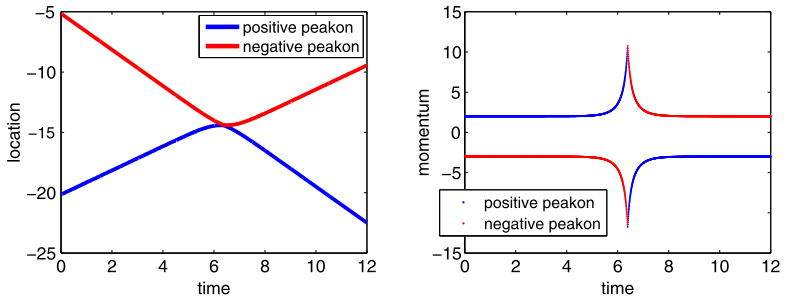

Fig. 11. Location and momentum trajectories for the peakon–antipeakon (with different magnitudes) interaction.

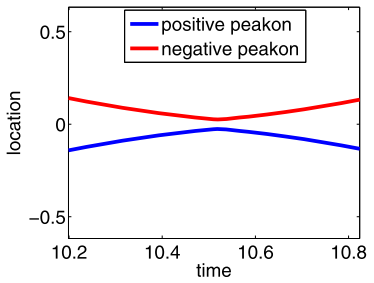

Fig. 12. (Zoomed) Location trajectories for the peakon–antipeakon (with different magnitudes) interaction.

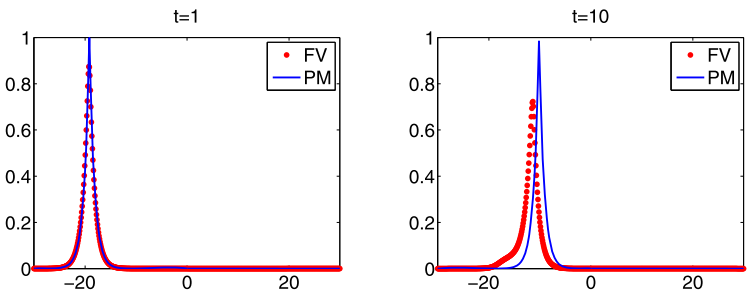

Fig. 13. The single peakon solution obtained by both PM and FV at times $t = 1, 10$ with $N_p = N_c = 500$.

[24]). The obtained results demonstrate the advantages that the particle method holds over the finite-volume method. In all of the examples that follow, we take $\alpha = 1$.

4.1. Peakon initial data

4.1.1. Single peakon

We begin by considering a single peakon solution and first implement the multi-particle approach described in Section 3.1.1 in the context of two particles. To this extent, we place $N_p = 500$ equidistant particles in the interval $[-30, 30]$ at $t = 0$ such that $p_i = 0$ for $i \neq q$ and $p_q = 1$. As we discussed before, the weights of all of the zero particles in consideration will remain constant in time. Their locations will change in time according to the values of the velocity $u(x_i(t), t)$, which in this case depends solely on $x_q(t)$ and $p_q(0)$, and therefore can be computed explicitly:

$$u\big(x_i(t), t\big) = \frac{1}{2} p_q(t) e^{-|x_q(t) - x_i(t)|}, \quad x_q(t) = \frac{1}{2} p_q(0) t + x_q(0). \tag{19}$$

This remarkable simplicity in integrating the ODE as well as recovering the solution at any $t > 0$ is one advantage that the particle method holds over say a finite volume approach. To illustrate this, we compare the results generated from the particle method to those obtained by applying a semi-discrete second-order central-upwind scheme described in Appendix A to the CH equation (1). In the finite volume setting, we use a uniform grid $x_j = j\Delta x^c$ with $\Delta x^c = 0.12$ (i.e., $N_c = 500$) on the same interval $[-30, 30]$. To compare the FV solution with the PM solution we run the simulations until $t = 1$ and $t = 10$ (initially we place particles at the middle of each finite volume cell). The solutions obtained by both methods are presented in Fig. 13. As one can see, the particle solution generates a more accurate approximation the solution of (1) due to the minimal effects of numerical diffusion. We observe that the maximum height of the "peak" generated from

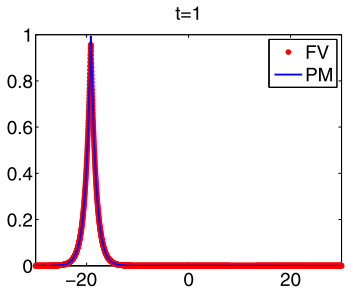

Fig. 14. The single peakon solution obtained by both PM and FV at times $t = 1$ with $N_p = 500$, $N_c = 3000$.

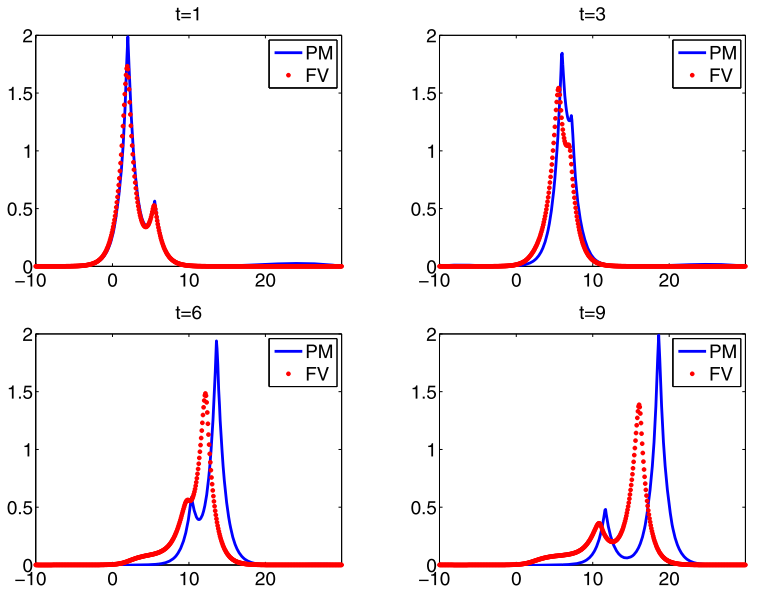

Fig. 15. The velocity u for the CH equation obtained by FV and PM at various times with $N_p = N_c = 500$.

the central-upwind scheme becomes noticeably smaller as time progresses. This is due to the numerical diffusion introduced by the finite volume method which is a result of its Eulerian nature. In contrast, the particle method is Lagrangian in nature, and hence is generally resistant to the numerical diffusion introduced in the approximation of the solution. In Fig. 14 we show that the FV solution converges to the particle solution through an appropriate grid refinement study. In this figure, we take $N_c = 3000$ in the FV simulations while the number of particles remains $N_p = 500$ as before.

Remark 1. We would like to remark that the examples considered in this paper are comparable with [30], in which they solved the CH equation with both peakon initial data and non-peakon initial data. There, they considered a local discontinuous Galerkin method to numerically solve the CH equation.

4.1.2. Two peakons

Next, we return to the two-peakon problem discussed in Section 3.1.1 and perform a comparison against a central-upwind scheme. Similar to the previous example, for the finite volume method, we use a uniform grid $x_j = j\Delta x^c$ with $\Delta x^c = 0.12$ (i.e., $N_c = 500$) on the same interval $[-10, 30]$. Similar to the one peakon case, we see in Fig. 15 that the peak associated with the FV solution is shorter than that of the PM solution which is a direct consequence of the numerical diffusion introduced into the problem. Due to this dampening of the peakon's height from the finite volume method, we expect that as the peakons propagate in time, the error between the central-upwind scheme and particle method grows. One can reduce this error between the simulations by considering a finer computational grid for the central-upwind scheme. In Fig. 16, we consider such a refinement by taking $N_c = 2000$ while still having $N_p = 500$. This shows that the particle method is able to capture complicated nonlinear interactions among peakon solutions for (1) with considerably fewer points compared to finite volume methods. We also see that as in the single peakon example, the solution generated from the finite volume method will converge to the particle method.

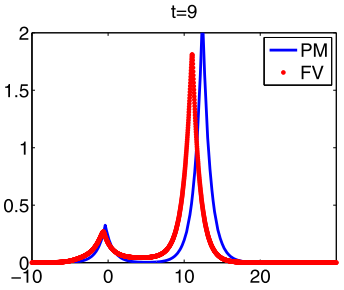

Fig. 16. The velocity u for the CH equation at $t = 9$ with $N_p = 500$, $N_c = 2000$.

4.2. Arbitrary smooth initial data

If we do not consider an initial condition in the form of a linear combination of peakon solutions, then we are no longer guaranteed that the particle method will yield an exact solution to (1). To this extent, we consider the following smooth initial data:

$$m(x,0) = \begin{cases} 3\cos^2(\frac{1}{4}x), & |x| \leqslant \pi, \\ 0, & |x| > \pi. \end{cases} \tag{20}$$

To simulate solutions using a particle method, we place $N_p = 500$ equidistant particles in the interval $[-10, 30]$ at $t = 0$, with the initial weights given by $p_i(0) = \Delta x^p m(x_i(0), 0)$ where $\Delta x^p = \frac{4}{50}$. We then evolve the locations and weights if the particles according to the system of ODEs given by (4). As usual, we recover the velocity $u(x,t)$ at some final time t by computing its values on a uniform grid according to (6) (here we take the same Δx^p used in the initial placement of the particles). To simulate solutions via a semi-discrete central-upwind scheme, we use a uniform grid $x_j = j\Delta x^c$ with $\Delta x^c = \Delta x^p$ on the same interval $[-10, 30]$. For clarity purposes, at further times ($t > 4$), we extend the computation domain so that one may clearly see the "peakon train" that forms as we simulate the solution for longer periods of time.

In Fig. 17, we show that the PM solution generates a more accurate approximation of the solution of (1) due to its low numerical diffusion. We observe a "steepening behavior" as was described in [4,5] and the formation of peakons from arbitrarily smooth data. This is due to the complete integrability of (1). In fact, we expect peakons to form after a finite time for any smooth arbitrary initial data.

The accuracy of both the particle and finite volume method may be visualized by performing a grid refinement study as is done in Fig. 18. Similar to the peakon simulations in Section 4.1, we observe that the maximum height of the "peak" generated from the central-upwind scheme becomes noticeably smaller as time progresses. Finally, in Fig. 19, we show that the FV solution converges to the PM solution with a suitably refined grid. Here we consider $N_c = 7000$ compared to the original $N_p = 500$ particles placed in a uniform grid for the particle method. This shows once again that the particle method is able to better resolve the solution to (1) under a suitable class of smooth initial data, with less points than a finite volume method.

5. Grid refinement analysis/accuracy test

Recalling that (1) admits traveling wave solutions of the form

$$u(x,t) = ce^{-|x-ct|}, \tag{21}$$

if we assume that the initial condition associated with (1) is of the form of a single peakon, then (1) assumes this traveling wave solution. To test the accuracy of our methods, we would like to perform a grid refinement study on both the particle method and semi-discrete central upwind scheme applied to (1). To begin, we follow the methods of [30] by considering a periodized version of (21). To this extent, we consider (21) coupled with the following initial condition

$$u_0(x) = \begin{cases} \frac{c}{\cosh(a/2)}\cosh(x - x_0), & |x - x_0| \leqslant a/2, \\ \frac{c}{\cosh(a/2)}\cosh(a - (x - x_0)), & |x - x_0| > a/2, \end{cases} \tag{22}$$

to get the exact solution $u(x,t) = u_0(x - t)$. Here, x_0 is the position of the trough and a is the period. The following simulations were ran with $c = 1$, $a = 30$, $x_0 = -5$. The computation domain is taken to be $[0, a]$. We begin with a grid refinement analysis for the particle method. Below are the results for $t = 1$ (Table 1). A grid refinement analysis for the semi-discrete central upwind scheme applied to (1) is given below (Table 2). From table, we see that once again, we have a first order accurate numerical scheme.

We note that the absolute error for the particle method is far better than the semi-discrete central upwind scheme (FV) scheme, although the rate of the convergence seems to vary between 1 and 2. This is the result of the low regularity associated with the peakon solution for the CH equation.

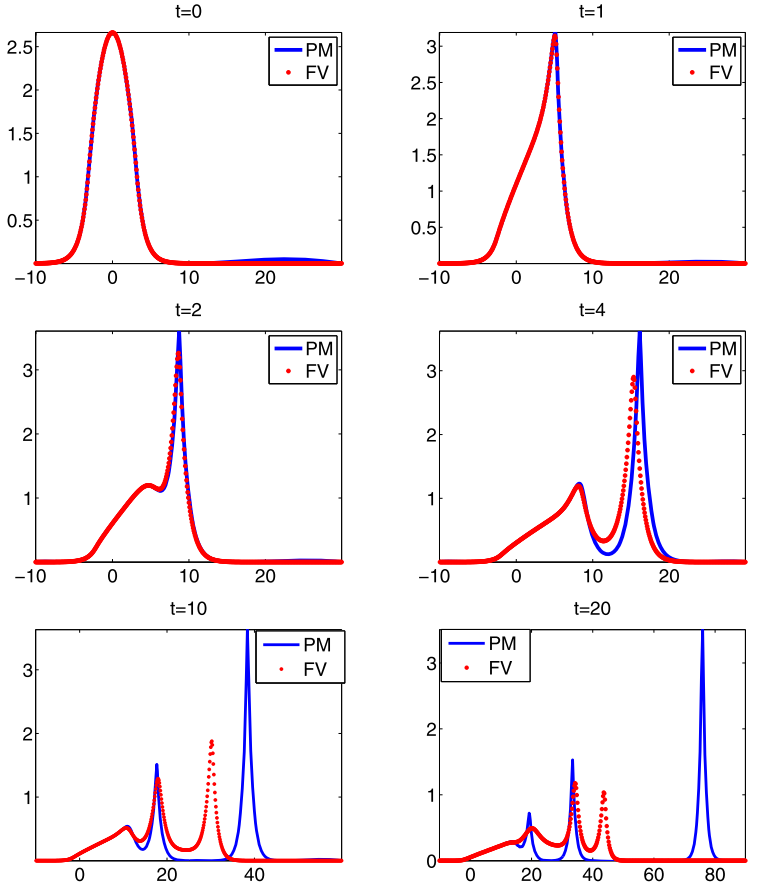

Fig. 17. The velocity u for the CH equation obtained by FV and PM at various times with $N_c = N_p = 500$.

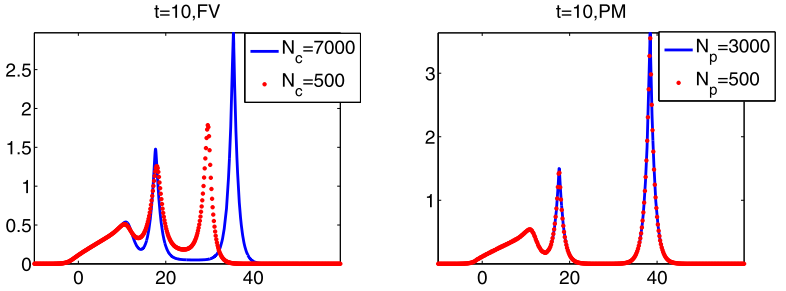

Fig. 18. A comparison of the velocity u for the CH equation obtained by FV and PM at $t = 10$.

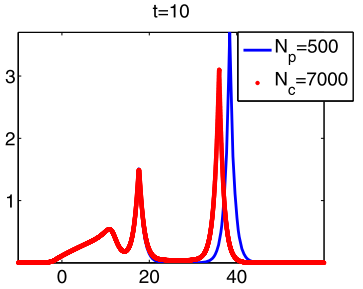

Fig. 19. The velocity u for the CH equation obtained by FV and PM at $t = 10$, $N_c = 7000$ and $N_p = 500$.

Table 1
Grid refinement analysis, $\|u(x,t) - u_{PM}(x,t)\|$.

N	L_2	Ratio	L_∞	Ratio
100	2.1511e−05	N/A	1.4397e−05	N/A
200	3.0512e−05	1.42	1.5501e−05	1.08
400	4.3157e−05	1.41	1.6088e−05	1.04
800	6.1017e−05	1.41	1.6392e−05	1.02
1600	8.6272e−05	1.41	1.6546e−05	1.01

Table 2
Grid refinement analysis, $\|u(x,t) - u_{CU}(x,t)\|$.

N	L_2	Ratio	L_∞	Ratio
100	0.2688	N/A	0.1484	N/A
200	0.2380	1.13	0.1307	1.14
400	0.2169	1.10	0.0835	1.56
800	0.1687	1.29	0.0595	1.40
1600	0.1493	1.13	0.0362	1.64

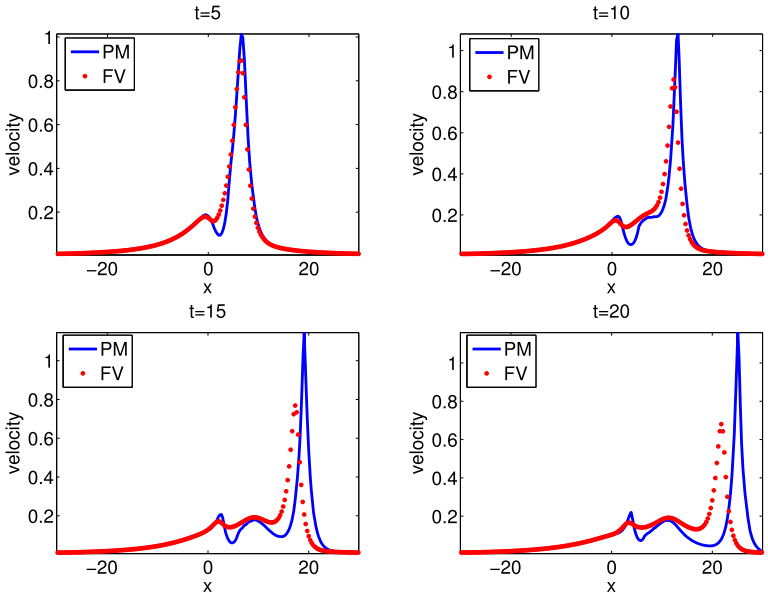

Fig. 20. The velocity u for the CH equation obtained by FV and PM at various times with $N_c = N_p = 200$.

5.1. A solution with a discontinuous derivative

In this section, we follow [30,20] by considering an initial condition for the velocity u which has a discontinuous derivative. In what follows, we solve (1) subject to the initial condition (for u):

$$u_0(x) = \frac{10}{(3+|x|)^2}. \tag{23}$$

Though we are given $u_0(x) = u(x,0)$, we may easily recover $m(x,0) = u(x,0) - u_{xx}(x,0)$ using a second order central finite difference scheme to approximate $u_{xx}(x,0)$. Once $m(x,0)$ is known, we apply a particle method to (1) with the initial condition $m(x,0)$ in a similar manner as was done for the example which considered arbitrary smooth data as an initial condition for $m(x,0)$. That is, we place $N_p = 200$ equidistant particles in the interval $[-30,30]$ at $t = 0$, with the initial weights given by $p_i(0) = \Delta x^p m(x_i(0),0)$ where $\Delta x^p = \frac{3}{10}$. We then evolve the locations and weights if the particles according to the system of ODEs given by (4). Similarly to the previous examples, we recover the velocity $u(x,t)$ at some final time t by computing its values on a uniform grid according to (6) (as usual we take the same Δx^p used in the initial placement of the particles). To simulate solutions via a semi-discrete central-upwind scheme, we use a uniform grid $x_j = j\Delta x^c$ with $\Delta x^c = \Delta x^p$ on the same interval $[-30,30]$.

In Fig. 20, we show that the PM solution generates a more accurate approximation the solution of (1) due to low of numerical diffusion. We also compare the resolution of our solution with that obtained in [20] and [30]. In [20], they

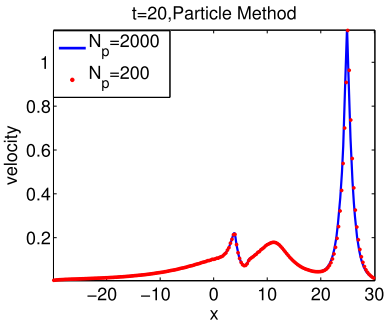

Fig. 21. The velocity u for the CH equation obtained by FV and PM at $t = 20$ with $N_p = 200$ and $N_p = 2000$.

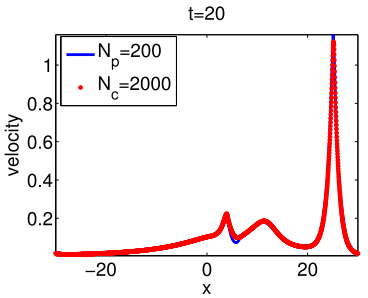

Fig. 22. The velocity u for the CH equation obtained by FV and PM at $t = 20$ with $N_c = 2000$ and $N_p = 200$.

consider a numerical scheme for which the solution to (1) is approximated with a sequence of multi-peakons. Here the solution was computed with a very high resolution ($n = 100$ peakons over the computational domain $[-30, 30]$). In [30], the solution to (1) is computed using a local discontinuous Galerkin method (LDG). Here the solution is computed using quadratic polynomials with $n = 640$ cells. Using only $n = 200$ particle methods we are able to obtain a good resolution of the solution comparable with that in [20,30]. In fact, in Fig. 21, we show that if one considers using more particles (say $n = 2000$), then the differences among the two solutions are visually negligible. Finally in Fig. 22, we show that by using considering more grid points in the semi-discrete central upwind scheme, we may obtain a reasonable resolution for the solution.

Remark 2. We would like to remark that in [20], the authors discussed a Lagrangian coordinate reformulation of the CH equation which led to a new ODE system for the evolution of the multi-peakon solution for the CH equation. Similarly to the results obtained in this paper, peakons also do not cross each other in their approach.

6. Conclusion

In this paper, we applied a particle method to the CH equation (1) to show that the nonlinear interaction among peakon solutions for (1) is indeed an elastic collision. This was accomplished by using the conservation of momentum and conservation of kinetic energy associated with the particle system obtained from the particle method applied to the considered equations. We were able to visualize these results through a numerical implementation of the method. Furthermore, we were able to explicitly showcase some of the advantages a particle method holds over other numerical methods, such a semi-discrete central upwind scheme, in simulating these solutions. For instance, the particle method allowed us to show multiple solutions for the peakon–antipeakon interaction for the CH equation. We were also able to show that the particle method can capture the interaction and dynamics of the solution with a lower resolution than a semi-discrete central upwind method.

To this extent, we have only provided an analytical and theoretical study of the dynamics and interaction of peakon solutions for (1). In the future, numerical experiments will performed on the analogous 2-D version of (1) more commonly referred to as the EPDiff equation with arbitrary initial data. We will also analyze the interaction and dynamics of peakon solutions generated from numerically solving the EPDiff equation.

Acknowledgements

The work of A. Chertock and T. Pendleton was supported in part by the NSF Grants DMS-1115682 and DMS-1216974 and the ONR Grant N00014-12-1-0832; the work of J.-G. Liu was supported in part by the NSF Grant DMS 10-11738. The authors also acknowledge the support by the NSF RNMS grant DMS-1107444.

Appendix A. Central upwind scheme for the CH equation

In this section, we briefly describe a semi-discrete second-order central-upwind scheme used for numerical solution of the CH equation (1). For additional details we refer the reader to [24].

To implement the semi-discrete scheme for the CH equation, we first rewrite the equation in the equivalent conservative form:

$$m_t + f(m,u)_x = 0, \tag{A.1}$$

where the flux function f is defined as follows:

$$f(m,u) := um + \frac{1}{2}u^2 - \frac{\alpha^2}{2}u_x^2, \quad m = u - \alpha^2 u_{xx}. \tag{A.2}$$

We divide the computational domain into the cells $C_j = [x_{j-\frac{1}{2}}, x_{j+\frac{1}{2}}]$ of size Δx^c with $x_j = j\Delta x^c$, where Δx^c is a small spatial scale assumed, for simplicity, to be a constant. We then denote the cell averages of m by

$$\overline{m}(t) := \frac{1}{\Delta x^c}\int\limits_{C_j} m(x,t)\,dx, \tag{A.3}$$

integrate (A.1) over cell C_j and divide both sides by Δx to obtain

$$\frac{d}{dt}\overline{m}_j(t) + \frac{f(m,u)|_{x_{j+\frac{1}{2}}} - f(m,u)|_{x_{j-\frac{1}{2}}}}{\Delta x^c} = 0. \tag{A.4}$$

The derivation of the scheme will be complete once the fluxes at the cell interfaces in (A.4) are approximated numerically, that is, the numerical fluxes $H_{j\pm\frac{1}{2}}(t) \approx f(m,u)|_{x_{j\pm\frac{1}{2}}}$ are constructed.

We follow [24] and compute the numerical fluxes according to the central-upwind approach. Namely, for a particular choice of time, say $t = t^n$, we consider (A.4), coupled with a piecewise polynomial initial condition

$$\widetilde{m}(x,t^n) = \mathcal{P}_j(x), \quad x \in C_j, \tag{A.5}$$

obtained from the cell averages available at $t = t^n$. It should be observed that the order of accuracy of the method will depend on the order of accuracy of the piecewise polynomial reconstruction in (A.5). For instance, for the second-order scheme, one may use the following piecewise linear polynomial reconstruction:

$$\mathcal{P}_j(x,t) = \overline{m}_j(t) + (m_x)_j(x - x_j), \quad x \in C_j. \tag{A.6}$$

For the resulting scheme to be non-oscillatory, one must use a nonlinear limiter when computing the numerical derivatives $(m_x)_j$ in (A.6). For instance, one may use

$$(m_x)_j = \operatorname{minmod}\left(\theta\frac{\overline{m}_j - \overline{m}_{j-1}}{\Delta x^c}, \frac{\overline{m}_{j+1} - \overline{m}_{j-1}}{2\Delta x^c}, \theta\frac{\overline{m}_{j+1} - \overline{m}_j}{\Delta x^c}\right), \tag{A.7}$$

where $1 \leqslant \theta \leqslant 2$ and

$$\operatorname{minmod}(z_1, z_2, \ldots) := \begin{cases} \min_j\{z_j\}, & z_j > 0\ \forall j, \\ \max_j\{z_j\}, & z_j < 0\ \forall j, \\ 0, & \text{otherwise.} \end{cases} \tag{A.8}$$

In our numerical simulations, we used $\theta = 1.5$.

Given a piecewise polynomial reconstruction (A.6), we compute the point values go the solution m at each cell interface, i.e.,

$$m^+_{j+1/2} := \mathcal{P}_{j+1}(x_{j+1/2}) \quad \text{and} \quad m^-_{j+1/2} := \mathcal{P}_j(x_{j+1/2}),$$

where $x_{j\pm1/2} = x_j \pm \frac{\Delta x^c}{2}$.

It should be observed that there may exist discontinuities at the end points for each value of j in our linear piecewise polynomial reconstruction. These possible discontinuities propagate with right- and left-sided local speeds, which may be estimated as follows

$$a^+_{j+1/2} = \max\{u^-_{j+1/2}, u^+_{j+1/2}, 0\},$$
$$a^-_{j+1/2} = \min\{u^-_{j+1/2}, u^+_{j+1/2}, 0\},$$

where $u^\pm_{j+1/2}$ are the values of the velocities at cell interfaces. We recall that the momentum and velocity in the CH equation (1) are related through the modified Helmholtz equation, which we solve by implementing a Fast Fourier Transform at each time step in order to recover the required values of u.

According to [24], the second-order semi-discrete central-upwind scheme is then given as

$$\frac{d}{dt}\overline{m}_j(t) = -\frac{H_{j+1/2}(t) - H_{j-1/2}(t)}{\Delta x^c}, \tag{A.9}$$

where the numerical fluxes, $H_{j+1/2}$, are

$$H_{j+1/2}(t) = \frac{a^+_{j+1/2} f(m^-_{j+1/2}) - a^-_{j+1/2} f(m^+_{j+1/2})}{a^+_{j+1/2} - a^-_{j+1/2}} + \frac{a^+_{j+1/2} a^-_{j+1/2}}{a^+_{j+1/2} - a^-_{j+1/2}}\left[m^+_{j+1/2} - m^-_{j+1/2}\right]. \tag{A.10}$$

We remark that the resulting scheme (A.9), (A.10) is a system of time dependent ODEs which should be solved using a high-order (at least second order accuracy) method. For our numerical experiments, we used a third-order SSP (strong stability preserving) Runge–Kutta method (see e.g. [19]) with adaptive time step $\Delta t < \frac{\Delta x^c}{2a_{\max}}$, where

$$a_{\max} := \max_j\{a^+_{j+1/2}, -a^-_{j+1/2}\}.$$

References

[1] R. Artebrant, H. Schroll, Numerical simulation of Camassa–Holm peakons by adaptive upwinding, Appl. Numer. Math. 56 (5) (2006) 695–711.
[2] R. Camassa, D. Holm, An integrable shallow water equation with peaked solitons, Phys. Rev. Lett. 71 (11) (1993) 1661–1664.
[3] R. Camassa, L. Lee, A completely integrable particle method for a nonlinear shallow-water wave equation in periodic domains, in: Advances in Dynamical Systems, Dyn. Contin. Discrete Impuls. Syst. Ser. A Math. Anal. 14 (S2) (2007) 1–5.
[4] R. Camassa, D. Holm, J. Hyman, A new integrable shallow water equation, Adv. Appl. Mech. 31 (1994) 1–33.
[5] R. Camassa, J. Huang, L. Lee, On a completely integrable numerical scheme for a nonlinear shallow-water wave equation, J. Nonlinear Math. Phys. 12 (1) (2005) 146–162.
[6] R. Camassa, J. Huang, L. Lee, Integral and integrable algorithms for a nonlinear shallow-water wave equation, J. Comput. Phys. 216 (2) (2006) 547–572.
[7] A. Chertock, A. Kurganov, On a practical implementation of particle methods, Appl. Numer. Math. 56 (2006) 1418–1431.
[8] A. Chertock, D. Levy, Particle methods for dispersive equations, J. Comput. Phys. 171 (2) (2001) 708–730.
[9] A. Chertock, D. Levy, A particle method for the KdV equation, J. Sci. Comput. 17 (2002) 491–499.
[10] A. Chertock, P. Du Toit, J. Marsden, Integration of the EPDiff equation by particle methods, M2AN, Math. Model. Numer. Anal. 46 (2012) 515–534.
[11] A. Chertock, J.-G. Liu, T. Pendleton, Convergence of a particle method and global weak solutions of a family of evolutionary PDEs, SIAM J. Numer. Anal. 50 (1) (2012) 1–21, http://dx.doi.org/10.1137/110831386.
[12] P.H. Chiu, L. Lee, T.W.H. Sheu, A dispersion-relation-preserving algorithm for a nonlinear shallow-water wave equation, J. Comput. Phys. 228 (21) (2009) 8034–8052.
[13] D. Cohen, B. Owren, X. Raynaud, Multi-symplectic integration of the Camassa–Holm equation, J. Comput. Phys. 227 (11) (2008) 5492–5512.
[14] A. Constantin, B. Kolev, On the geometric approach to the motion of inertial mechanical systems, J. Phys. A, Math. Gen. 35 (2002) R51–R79.
[15] A. Constantin, B. Kolev, Geodesic flow on the diffeomorphism group of the circle, Comment. Math. Helv. 78 (2003) 787–804.
[16] A. Constantin, W.A. Strauss, Stability of peakons, Commun. Pure Appl. Math. 53 (5) (2000) 603–610.
[17] K. El Dika, L. Molinet, Exponential decay of H^1-localized solutions and stability of the train of N solitary waves for the Camassa–Holm equation, Philos. Trans. R. Soc., Math. Phys. Eng. Sci. 365 (1858) (2007) 2313–2331.
[18] B.-F. Feng, K.-i. Maruno, Y. Ohta, A self-adaptive moving mesh method for the Camassa–Holm equation, J. Comput. Appl. Math. 235 (1) (2010) 229–243.
[19] S. Gottlieb, C.-W. Shu, E. Tadmor, Strong stability-preserving high-order time discretization methods, SIAM Rev. 43 (2001) 89–112.
[20] H. Holden, X. Raynaud, A convergent numerical scheme for the Camassa–Holm equation based on multipeakons, Discrete Contin. Dyn. Syst. 14 (3) (2006) 505–523.
[21] D. Holm, T. Schmah, C. Stoica, Geometric Mechanics and Symmetry, Oxford Texts in Applied and Engineering Mathematics, vol. 12, Oxford University Press, Oxford, 2009.
[22] H. Kalisch, J. Lenells, Numerical study of traveling-wave solutions for the Camassa–Holm equation, Chaos Solitons Fractals 25 (2) (2005) 287–298.
[23] H. Kalisch, X. Raynaud, Convergence of a spectral projection of the Camassa–Holm equation, Numer. Methods Partial Differ. Equ. 22 (5) (2006) 1197–1215.
[24] A. Kurganov, S. Noelle, G. Petrova, Semidiscrete central-upwind schemes for hyperbolic conservation laws and Hamilton–Jacobi equations, SIAM J. Sci. Comput. 23 (3) (2001) 707–740, http://dx.doi.org/10.1137/S1064827500373413 (electronic).
[25] J. Lenells, Stability of periodic peakons, Int. Math. Res. Not. 10 (2004) 485–499.
[26] T. Matsuo, H. Yamaguchi, An energy-conserving Galerkin scheme for a class of nonlinear dispersive equations, J. Comput. Phys. 228 (12) (2009) 4346–4358.

[27] A. Newell, Solitons in Mathematics and Physics, CBMS-NSF Regional Conference Series in Applied Mathematics, vol. 48, Society for Industrial and Applied Mathematics (SIAM), Philadelphia, PA, 1985.
[28] P.-A. Raviart, An analysis of particle methods, in: Numerical Methods in Fluid Dynamics, Como, 1983, in: Lecture Notes in Math., vol. 1127, Springer, Berlin, 1985, pp. 243–324.
[29] G. Rocca, M. Lombardo, M. Sammartino, V. Sciacca, Singularity tracking for Camassa–Holm and Prandtl's equations, Appl. Numer. Math. 56 (8) (2006) 1108–1122.
[30] Y. Xu, C.-W. Shu, A local discontinuous Galerkin method for the Camassa–Holm equation, SIAM J. Numer. Anal. 46 (4) (2008) 1998–2021.